SPIN-WAVE EXCITATIONS IN Gd AT LOW TEMPERATURES

SPIN-WAVE EXCITATIONS IN Gd AT LOW TEMPERATURES

SPIN–WAVE EXCITATIONS IN Gd AT LOW TEMPERATURES

永田正一・宮崎雅年・藤田英司
戎　修二・山村秀美・谷口　哲

Shoich NAGATA, Masatosi MIYAZAKI, Eiji FUJITA
Shuji EBISU, Hidemi YAMAMURA and Satoshi TANIGUCHI

Abstract

It has been manifestly demonstrated that Gd is one of the best example to be realistically applied to the spin-wave theory of Heisenberg model for the localized magnetic moment.

The magnetization of Gd has been measured in the temperature $4<T<310$ K at a constant magnetic field of 6 kOe using a homemade vibrating sample magnetometer. We present an exact analysis of the spin-wave excitations for Gd. In the presence of an applied magnetic field, H, an energy gap exists in the spin-wave dispersion relation. As a consequence, the temperature dependence of the magnetization for ferromagnets must differ from the simple Bloch $T^{3/2}$ law. The low temperature magnetization per gram is found to obey the form: $\Delta\sigma(T)/\sigma(0)=BZ(3/2,T_g/T)T^{3/2}+CZ(5/2,T_g/T)T^{5/2}$, where B and C are constants and $\Delta\sigma(T)=\sigma(0)-\sigma(T)$. The modification factors $Z(3/2,T_g/T)$ and $Z(5/2,T_g/T)$ are the characteristic functions of T and the magnetic field, H. The spontaneous magnetization of ferromagnetic Gd follows $BZ(3/2,T_g/T)T^{3/2}$ relation (the modified Bloch $T^{3/2}$ law) with remarkable fidelity below 200 K.

1. Introduction

Ferromagnetic Gd metal has a Curie temperature of $T\sim293$ K and exhibits little single-ion anisotropy since its magnetic moment is produced almost wholly by spherically symmetric $^8S_{7/2}$ Gd^{3+} ions. Because its large magnetic moment is localized in the small $4f$ shell, Gd is, in principle, of more general validity for the spin-wave theory of Heisenberg model than the partially itinerant ferromagnets such as Fe and Ni.[1,2] However, much less information is available on the experimental study for the spin-wave excitations of Gd,[3-5] which motivated the present investigation.

We give an exact analysis of the spin-wave excitations in the presence of an applied magnetic field, H. It is seen that the energy gap due to the external magnetic field has a pronounced effect on the magnetization at lower temperatures. An energy gap exists in the spin-wave dispersion relation. As a consequence, the temperature dependence of the magnetization for ferromagnets must differ from the simple Bloch $T^{3/2}$ law. The low temperature magnetization per gram is found to obey the form:

$\Delta\sigma(T)/\sigma(0)=BZ(3/2,T_g/T)T^{3/2}+CZ(5/2,T_g/T)T^{5/2}$, where B and C are constants and $\Delta\sigma(T)$ is the decrease in the magnetization, $\Delta\sigma(T)=\sigma(0)-\sigma(T)$. The modification factors $Z(3/2,T_g/T)$ and $Z(5/2,T_g/T)$ are the characteristic functions of T and the magnetic field, H. These functions $Z(3/2,T_g/T)$ and $Z(5/2,T_g/T)$ have been calculated systematically.[6]

One can see that the ferromagnetic Gd proved directly the spin-wave excitations at low temperatures in accordance with the modified Bloch $T^{3/2}$ law. The best extrapolation to $T=0$ K at $H=6.00$ kOe gives $\sigma(0)=264$ (emu/g), which corresponds to $gJ=7.44$ Bohr magnetons/Gd-atom.[7] The source of the excess moment of 0.44 μ_B per Gd atom over the value of 7.00 μ_B arising from the seven unpaired $4f$ electrons has attracted significant theoretical attention.[8] In appendix, we will give some consideration on the subject of detection coil configurations for the Foner-type vibrating sample magnetometer from an analytical viewpoint.

2. Spin-Wave Excitations in a Constant Magnetic Field

In this section we describe briefly the spin-wave excitations in a constant magnetic field, in which the Bloch $T^{3/2}$ law should be modified as a consequence of the influence of the magnetic field.

In thermal equilibrium the number of magnon n_k excited at temperature T is given by the Bose distribution

$$<n_k>=1/\{\exp(\varepsilon_k/k_B T)-1\}\ , \tag{1}$$

where ε_k is the excitation energy of a spin wave of wave vector k. Since the total spin is reduced from its saturation value NS by one unit per spin wave, the magnetization per unit volume at temperature T satisfies

$$\begin{aligned} M(T)&=g\mu_B\{NS-\sum_k<n_k>\} \\ &=M(0)\{1-(1/NS)\sum_k<n_k>\}. \end{aligned} \tag{2}$$

This sum may be turned into an integral, and at low temperatures the Bose factor for large k is so small that the integral may safely be carried to infinity. Thus, for cubic lattice,

$$\frac{M(0)-M(T)}{M(0)}=\frac{g\mu_B}{M(0)(2\pi)^3}\int_0^\infty\frac{4\pi k^2}{\exp(\varepsilon_k/k_BT)-1}\mathrm{dk}, \tag{3}$$

where the integral extends over all k-space, multiplying by the $(1/2\pi)^3$ states available per unit volume of k-space in a unit volume of material.

In the absence of an applied magnetic field and the magnetocrystalline anisotropy, a general expansion appropriate to cubic symmetry for small k (the long–wave limit), is

$$\varepsilon_k = Dk^2 + Ek^4, \tag{4}$$

where D is the spin-wave stiffness constant and E is the constant of proportionality for the k^4 term. Making the substitution of eq. (4) into eq. (3), the magnetization per unit volume follows the Heisenberg-model prediction:[9]

$$\frac{\Delta M(T)}{M(0)} = \frac{M(0)-M(T)}{M(0)} = BT^{3/2} + CT^{5/2}, \tag{5}$$

where B and C are constants and the first term is the Bloch $T^{3/2}$ law, while the second one is due to higher-order term in the magnon dispersion relation. The coefficients of the corresponding terms in these equations are related through the expressions[9,10]

$$B = \zeta(3/2)[g\mu_B/M(0)](k_B/4\pi D)^{3/2} \tag{6}$$

and

$$C = \zeta(5/2)[g\mu_B/M(0)](k_B/4\pi D)^{5/2}(3\pi/4)\langle r^2\rangle, \tag{7}$$

where $\zeta(3/2)=2.612$ and $\zeta(5/2)=1.341$ are the Rieman ζ functions and $\langle r^2\rangle$ is the average mean-square range of the exchange interaction.

In the presence of an applied field H, on the other hand, the spin-wave dispersion relation for the long-wavelength limit ($k\sim 0$) is given by

$$\varepsilon_k = g\mu_B H + Dk^2 + Ek^4, \tag{8}$$

where $g\mu_B H$ is an energy gap. Here we introduce a gap temperature T_g,[1,2] defined by

$$T_g = g\mu_B H/k_B. \tag{9}$$

We obtain simply an expression for the magnetization if we neglect the k^4 term in the dispersion relation given by eq. (8).

$$\frac{M(0)-M(T)}{M(0)} = \frac{g\mu_B}{M(0)(2\pi)^3}\int_0^\infty \frac{4\pi k^2}{\exp[(Dk^2+k_BT_g)/k_BT)]-1}dk \tag{10}$$

$$= \frac{g\mu_B}{M(0)(2\pi)^3}\left(\frac{k_BT}{D}\right)^{3/2}\int_0^\infty \frac{4\pi q^2}{\exp(q^2+T_g/T)-1}dq. \tag{11}$$

The integration is to be carried out by

$$\int_0^\infty \frac{q^2}{\exp(q^2+T_g/T)-1}dq=\int_0^\infty q^2 dq \sum_{n=1}^{\infty}\exp[-n(q^2+T_g/T)] \tag{12}$$

$$=\sum_{n=1}^{\infty}\exp[(-n)T_g/T]\int_0^\infty[\exp(-n)q^2]q^2\,dq$$

$$=\sum_{n=1}^{\infty}\{[\exp((-n)T_g)][(\sqrt{\pi}/4)n^{-3/2}]\}$$
$$\equiv(\sqrt{\pi}/4)\zeta(3/2,T_g/T). \tag{13}$$

Then, we have

$$\frac{\Delta M(T)}{M(0)}=\frac{g\mu_B}{M(0)}\left(\frac{k_B}{4\pi D}\right)^{3/2}\zeta(3/2,T_g/T)T^{3/2}. \tag{14}$$

Because of the energy gap in eq. (8), eq. (5) must be modified and be described as eq. (14). The temperature dependence of the magnetization differs from the simple Bloch $T^{3/2}$ law under the influence of the magnetic field.

Furthermore, if we consider the k^4 term of eq. (8) in the dispersion relation, the modified version of eq. (5) is finally given by

$$\frac{\Delta M(T)}{M(0)}=BZ(3/2,T_g/T)T^{3/2}+CZ(5/2,T_g/T)T^{5/2}. \tag{15}$$

These coefficients of B and C are related to the spin-wave stiffness constant D and the average mean-square range $<r^2>$ of the exchange interaction given by eq. (6) and (7). The functions $Z(3/2,T_g/T)$ and $Z(5/2,T_g/T)$ can be written as

$$\zeta(3/2,T_g/T)=\zeta(3/2)Z(3/2,T_g/T), \tag{16}$$

$$\zeta(5/2,T_g/T)=\zeta(5/2)Z(5/2,T_g/T), \tag{17}$$

$$\zeta(a)=\sum_{n=1}^{\infty}n^{-a},\quad \zeta(3/2)=2.612,\quad \zeta(5/2)=1.341,$$

$$Z(3/2,T_g/T)=\frac{1}{\zeta(3/2)}\sum_{n=1}^{\infty}n^{-3/2}\quad\exp[(-n)T_g/T], \tag{18}$$

$$Z(5/2,T_g/T)=\frac{1}{\zeta(5/2)}\sum_{n=1}^{\infty}n^{-5/2}\quad\exp[(-n)T_g/T]. \tag{19}$$

These $Z(3/2,T_g/T)$, $Z(5/2,T_g/T)$ functions reduce to unity when T_g goes to zero. Namely, if there is no external magnetic field, the magnetization is immediately reduced to the eq. (5).

We give results of systematic calculations for the functions of $Z(3/2,T_g/T)$ and $Z(5/2,T_g/T)$.[6]

Figures 1 and 2 show the numerical results of these functions. The defining series (18) and (19) converge slowly at highr temperatures. Our computer calculations have been truncated if the numerical value had reached smaller quantity than 10^{-10}, for each temperature. As can be seen in Figs. 1 and 2, at lower temperatures the values of both Z functions become small, which reflects the important role of the magnetic field as a magnetic anisotropy. The stronger magnetic anisotropy makes to excite the less spin-waves. In each magnetic field, the magnitude of $Z(3/2, T_g/T)$ is

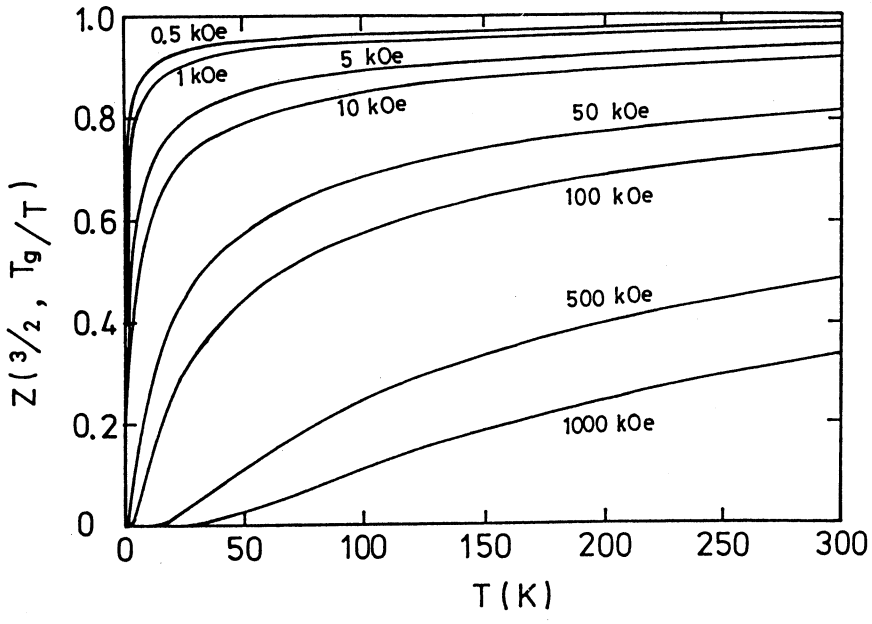

Fig. 1. The temperature variation of $Z(3/2, T_g/T)$ at various magnetic fields. T_g is defined by eq. (9), using $g=2.00$.

smaller than that of $Z(5/2, T_g/T)$.

At higher temperatures, in general, the spin-wave interactions become increasingly important and the T^4 term arises in eq. (5) as a consequence of this dynamical spin-wave interaction,[11] which is not discussed here.

3. Experimental Method

Polycrystalline small piece of sample $7 \times 7 \times 0.1$ mm^3 (99.9 % purity) was used with its plane parallel to the field in order to minimize the demagnetizing field effects.

The magnetization measurements were performed with a homemade vibrating sample magnetom-

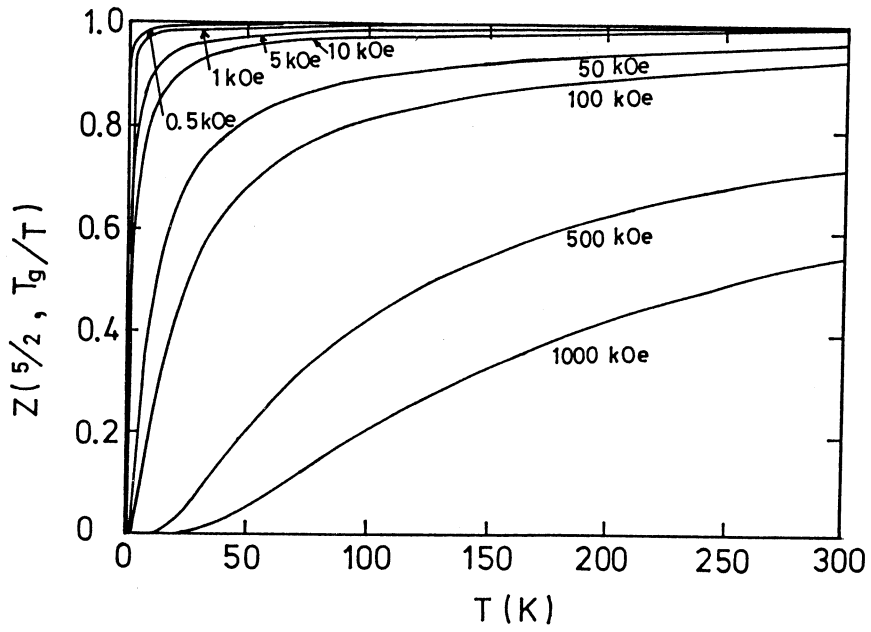

Fig. 2. The temperature variation of $Z(5/2, T_g/T)$ at various magnetic fields. T_g is defined by eq. (9), using $g=2.00$.

eter calibrated by pure nickel. The details about the apparatus which shows a setup of the cryostat and a measuring system of the magnetometer electronics, are given elsewhere.[12-14] Here, we show only a schematic representation of the mechanical arrangement for the homemade vibrating sample magnetometer in Fig. 3. In this paper, a new analysis of optimum design of a detection coil system for Foner-type vibrating sample magnetometer is given in Appendix.

The magnetization versus magnetic-field isotherms were taken at 5 K interevals from 4.2 to 310 K in a field up to 7.5 kOe. The magnetization as a function of temperature was also measured at a constant field of 6.00 kOe.

4. Experimental Results And Discussion

When one obtains a spontaneous magnetization of ferromagnets at a given temperature, the law of approach to saturation magnetization for the magnetization curve {extrapolating to $(1/H)=0$ or $H=0$} is used for actual measurements.[15] However in practical experiments, this process of the extrapolation sacrifices high precision of the evaluated values of the spontaneous magnetization. While, the temperature dependence of the magnetization at a constant field can be done fairly

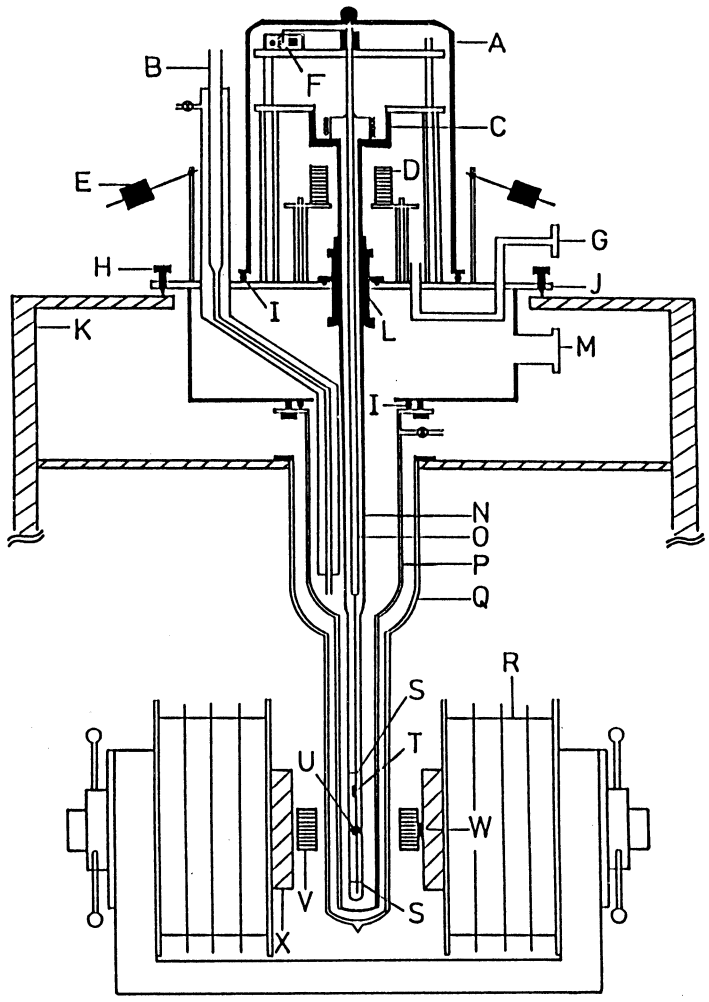

Fig. 3. Mechanical arrangement for the homemade vibrating sample magnetometer. (A) glass bell-jar, (B) liquid He transfer line, (C) speaker, (D) pick-up coils, (E) brass weight for vibration-damping, (F) amplitude detector(photodetection), (G) pumping line of sample chamber, (H) leveling screw, (I) O-ring seal, (J) base plate, (K) support bracket, (L) sample chamber centering guide attached to N, (M) He pumping line, (N) sample chamber, (0) sample support tube, (P) He Dewar, (Q) nitrogen Dewar, (R) magnet, (S) teflon spacer, (T) thermometer, (U) sample, (V) signal pick-up coils(four-coil detection system), (W) Hall sensor, (X) pole piece.

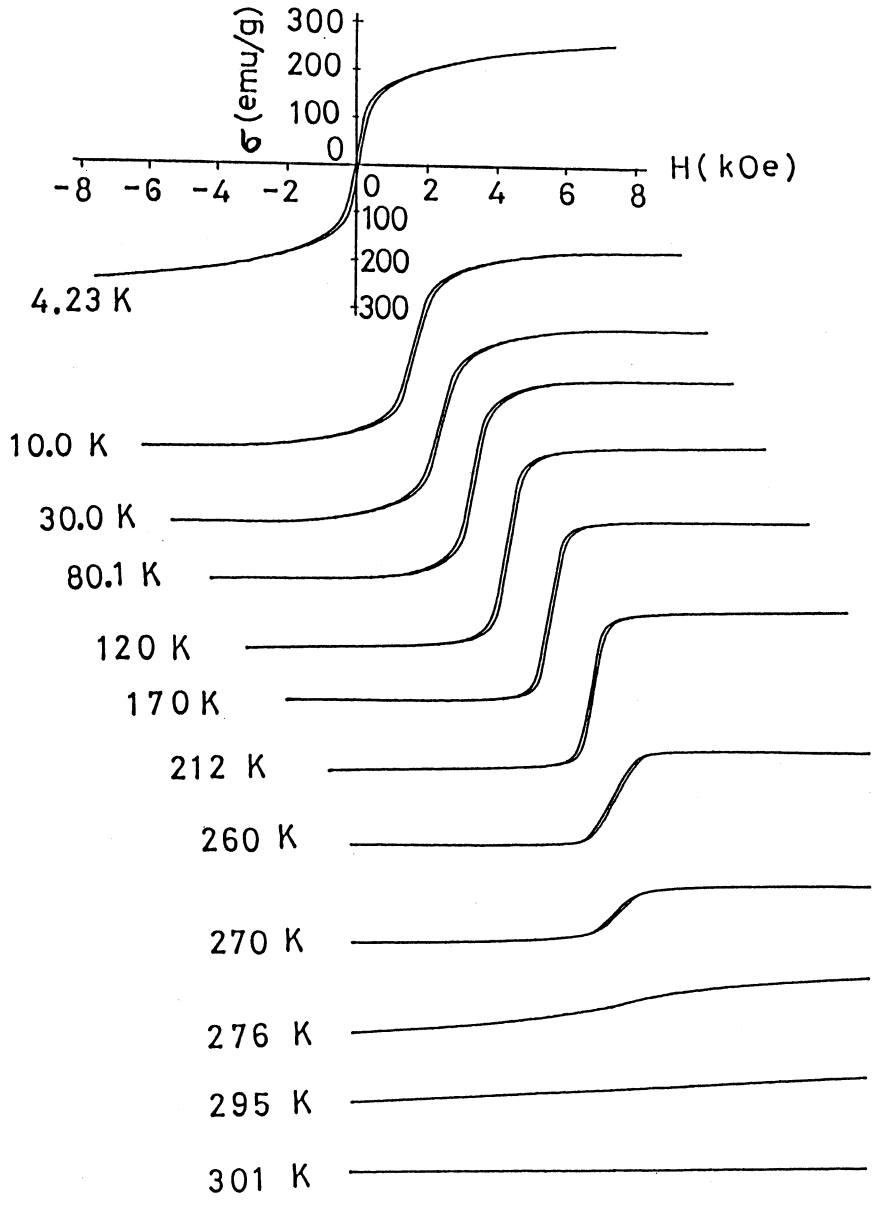

Fig. 4. Magnetization curves of Gd at various temperatures.

accurately.[7,10] However it should be noted that in the presence of the magnetic field, an increase of the magnetization itself is caused by the external magnetic field, in addition to Weiss molecular field. Under a moderately strong magnetic field, the excess magnetization forced by this external magnetic field is overlaped in the magnetization process. In a high field region, the forced-ferro magnetization remains as a function of the magnetic field in the almost saturated state. Consequently, we can determine carefully the magnitude of the magnetization at a constant magnetic field. Therefore, the spin-wave analysis in presence of the magnetic field, described in §2, is very important and useful for the analysis.

Because of our sample shape and the orientation to the applied magnetic field, demagnetizing effects are expected to be small. The magnetocrystalline anisotropy can be assumed to be also small for the $L=0$ state in Gd.[3] Therefore, no corrections were applied for the above two effects.

Figure 4 shows the magnetization curves up to 7.5 kOe. The magnetization versus magnetic-field isotherms were taken at 5 K intervals. The representative data of the temperature dependence of magnetization curves are shown. The temperature dependence of the magnetization at a constant magnetic field of 6.00 kOe is shown in Fig. 5.

It is easy to construct actual $Z(3/2,T_g/T)$ and $Z(5/2,T_g/T)$ functions on the theoretical ground described in §2. The numerical calculations of these Z-functions at $H=6.00$ kOe are given in Fig. 6. At lower temperatures these functions become seriously significant in eq. (15).

The assumption used in §2 that the spin-wave energy ε_k is given simply by eq. (8), is restricted to cubic lattice, while Gd has hexagonal lattice structure. Nevertheless, the simple analysis given in §2 is applied to Gd owing to a lack of the detailed knowledge for Gd at the present stage.

On the basis of the computer calcurations of Z-function in Fig. 6, Fig. 7 shows the results for $\Delta\sigma(T)/\sigma(0)$ vs $Z(3/2,T_g/T)T^{3/2}$ at the particular gap temperature T_g corresponding to $H=6.00$ kOe. One can find manifestly a straight line up to 200 K. The dominant $Z(3/2,T_g/T)T^{3/2}$ dependence can be clearly seen. The slope gives the spin-wave parameter B.

Realizing that besides the $Z(3/2,T_g/T)T^{3/2}$ contribution there exist $Z(5/2,T_g/T)T^{5/2}$ term in eq. (15), the next step of the analysis is to include $Z(5/2,T_g/T)T^{5/2}$ term. To show the evidence of the existence of the cofficient C, we plot $[Z(3/2,T_g/T)T^{3/2}]^{-1}$ $[\Delta\sigma(T)/\sigma(0)]$ versus $[Z(5/2,T_g/T)/Z(3/2,T_g/T)]$ T in Fig. 8 at the magnetic fleld of 6.00 kOe. From the intercept and the slope of the straight line, the spin-wave parameters B and C are determined. Below 50 K, the data points are very scattered as shown in Fig. 8.

Our experimental results are summarized as follows: (*a*) At temperatures below 200 K, $\Delta\sigma(T)$ is well represented by first $Z(3/2,T_g/T)T^{3/2}$ term clearly indicated in Fig. 7. (*b*) However, over

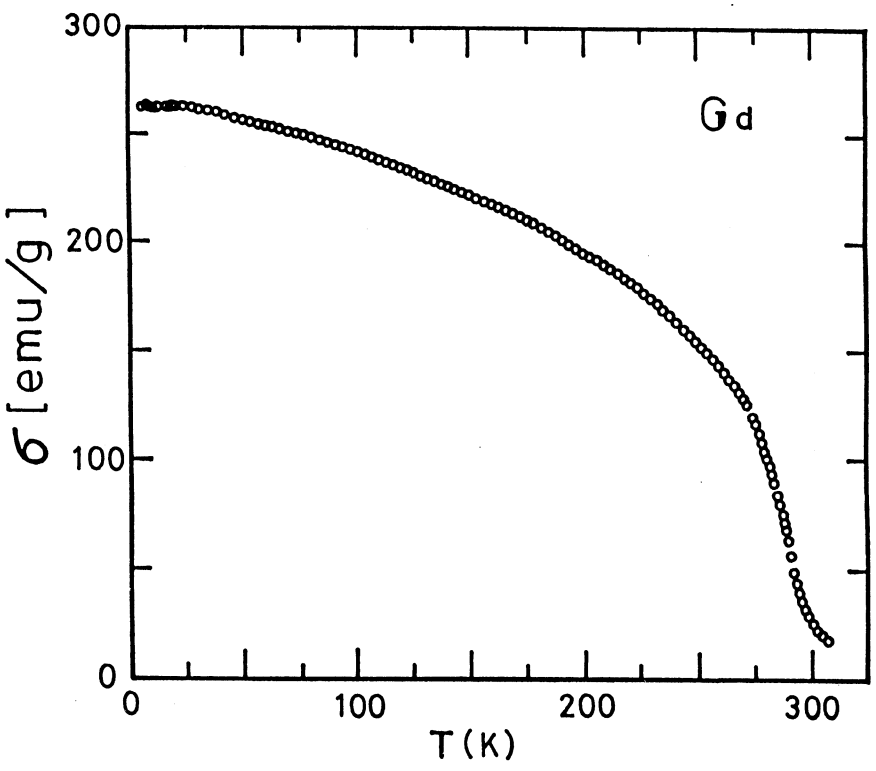

Fig. 5. The magnetization of Gd at H=6.00 kOe as a function of temperature.

wide temperature range below $T < 250$ K a much better representation is obtained by eq. (15) as shown in Fig. 8. (*c*) The spin-wave parameter B and C have been determined by a least-square fit:

$$B=(8.6\pm0.8)\times10^{-5} \quad (\mathrm{K}^{-3/2}), \tag{20}$$

$$C=(4.2\pm2.5)\times10^{-8} \quad (\mathrm{K}^{-5/2}). \tag{21}$$

Here the obtained value B from the results of Figs. 7 and 8 gives the same value within experimental errors. (*d*) The best extrapolation to $T=0$ K at $H=6.00$ kOe gives

$$\sigma(0)=264 \quad (\mathrm{emu/g}), \tag{22}$$

which corresponds to

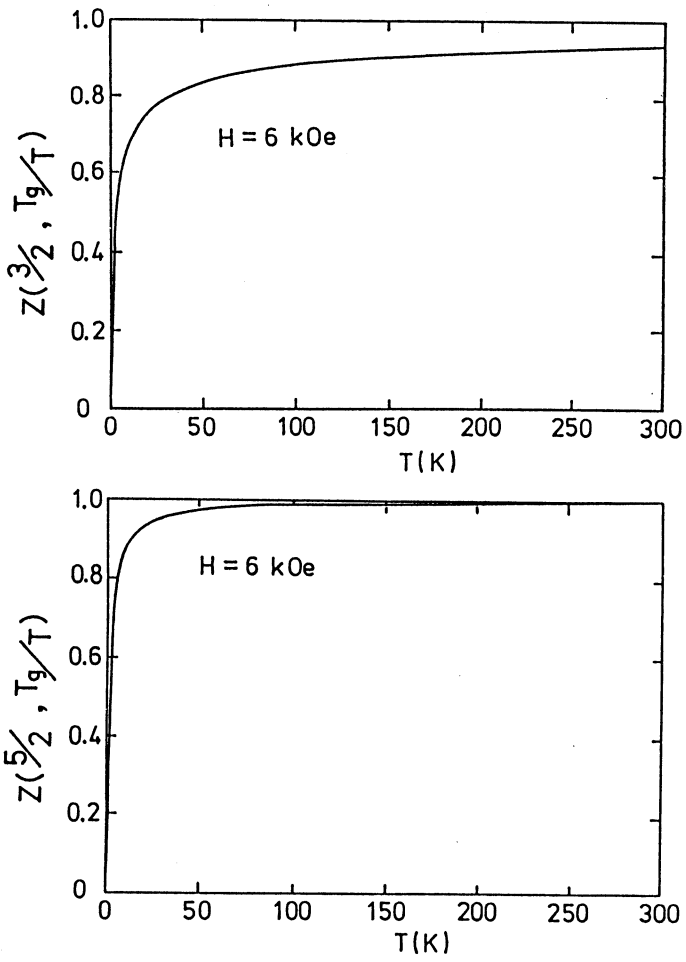

Fig. 6. Computer calculation of $Z(3/2,T_g/T)$ and $Z(5/2,T_g/T)$ at $H=6.00$ kOe as a function of temperature.

$$n_B=gJ=7.44(\mu_B/\text{Gd-atom}). \tag{23}$$

The source of the excess moment of 0.44 μ_B per Gd atom over the value of 7.00 μ_B arising from the seven unpaired $4f$ electrons has attracted significant theoretical attention. It is now attributed to the polarization of the conduction band electrons mediated by the localized $4f$ electrons via the exchange interaction.[8)]

As shown in Fig. 7, the magnetization follows modified Bloch $T^{3/2}$ law up to remarkably high temperature 200 K.[16)] Then the contribution of $T^{5/2}$ term to the magnetization becomes increasingly important at temperature higher than 200 K.

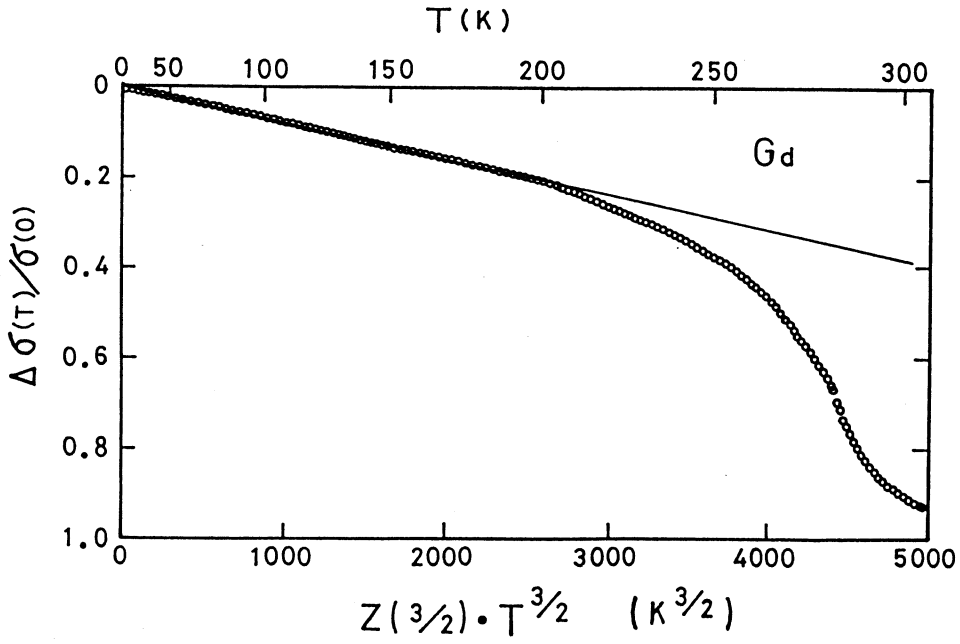

Fig. 7. $\Delta\sigma(T)/\sigma(0)$ vs $Z(3/2,T_g/T)^{3/2}$ at $H=6.00$ kOe.

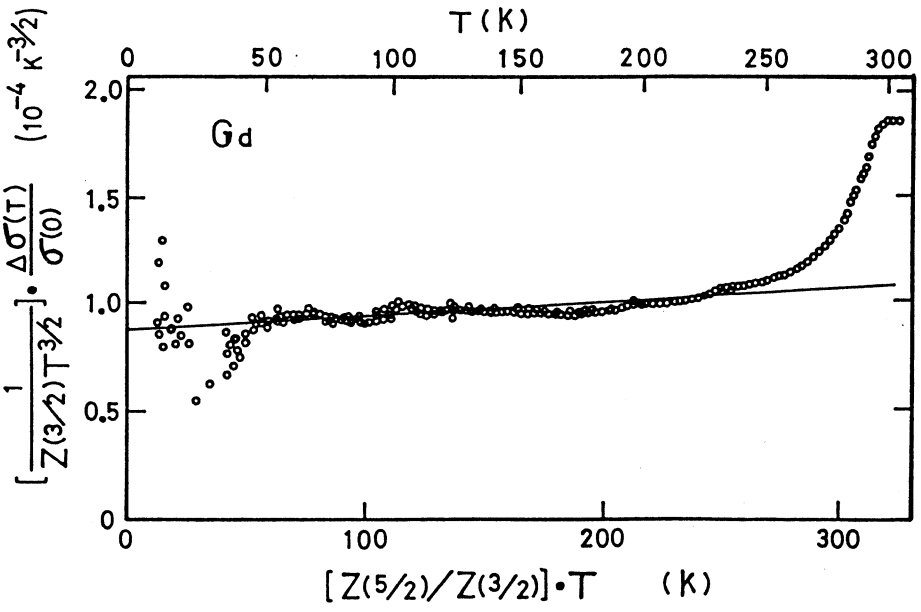

Fig. 8. $[Z(3/2,T_g/T)T^{3/2}]^{-1}\times[\Delta\sigma(T)/\sigma(0)]$ vs $[Z(5/2,T_g/T)/Z(3/2,T_g/T)]T$ at $H=6.00$ kOe.

5. Concluding Remarks

The low temperature magnetization per gram of Gd is found to obey the form:

$$\Delta\sigma(T)/\sigma(0)=BZ(3/2,T_g/T)T^{3/2}+CZ(5/2,T_g/T)T^{5/2}. \tag{24}$$

Below 200 K the dominant $BZ(3/2,T_g/T)T^{3/2}$ dependence can be clearly seen. The best extrapolation to $T=0$ K at $H=6.00$ kOe gives $\sigma(0)=264$ (emu/g), which corresponds to $n_B=gJ=7.44$ (μ_B/Gd–atom).

It has been manifestly demonstrated that Gd is the best example to be applied realistically to the spin-wave theory of Heisenberg model for the localized magnetic moment.

Appendix

A1. Optimum Design of Detection Coil System for Vibrating Sample Magnetometer

The optimum design of a detection coil system for Foner-type vibrating sample magnetometers is studied, which minimizes any undesirable influence due to sample mispositioning.[13]

The principle of the vibrating sample magnetometer can be understood with reference to the schematic drawing in Fig. A1. Consider a detection ciol (pick-up coil) consisting of a cross-sectional area S, of the number of turns N at point $A(x,y,z)$ sufficiently far away from the sample having a magnetic moment M located at the origin. The voltage V induced in the coil is

$$V=-N\mu_0 S dH_z(t)/dt, \tag{A1}$$

where μ_0 is the permeability of vacuum, and $H_z(t)$ is the z–component of the magnetic field created by the dipole moment M of the small sample vibrating along the z–axis. The magnetic potential ϕ_m at point A generated by the sample is given by

$$\phi_m=(Mx)/(4\pi\mu_0 r^3). \tag{A2}$$

Writing out the magnetic potentials at $t=0$ and $t=t$, we have

$$\phi_m(0)=(Mx)/(4\pi\mu_0 r^3)$$

and

$$\phi_m(t)=(Mx)/[4\pi\mu_0(r+\Delta r(t))^3]$$

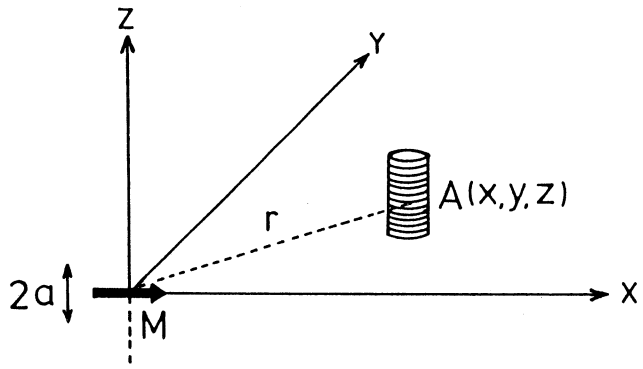

Fig. A1 The principle of a vibrating magnetometer based on Faraday's law. A magnetic moment M, which is aligned along the x-axis by an applied magnetic field, is vibrated along the z-axis at an angular frequency ω with an amplitude of a. The voltage is induced by a time-varying magnetic flux in a detection coil at the point $A(x,y,z)$. The axis of the detection coil is parallel to the direction of vibration of the sample.

$$=(Mx)/(4\pi\mu_0 r^3)\cdot\ [1-(3\Delta r(t))/r]. \qquad (A3)$$

Therefore, the part of $\phi_m(t)$ which varies with time is

$$\phi_m'(t)=-[(3Mx)/(4\pi\mu_0 r^4)]\Delta r(t). \qquad (A4)$$

For the motion of the magnetic moment M described by

$$\delta=(a)\cdot\cos(\omega t), \qquad (A5)$$

$\Delta r(t)$ approximately gives the value $\Delta r(t)=(z/r)\delta(t)$ for a sufficiently small displacement δ from the mean sample position. Then, the $\phi_m'(t)$ leads to

$$\phi_m'(t)=-[(3Mxz)/(4\pi\mu_0 r^5)](a)\cos(\omega t), \qquad (A6)$$

and the z-component of the magnetic field, $H_z(t)$, at point A is given by

$$H_z(t)=-\mathrm{d}\phi_m'(t)/\mathrm{dz}$$

$$=[(3aMx)/(4\pi\mu_0)]\cdot[(1/r^5)-(5z^2)/r^7]\cos(\omega t). \qquad (A7)$$

Let us now take the mean position of the detection coil as $A(x,y,0)$; hence, the value of $(5z^2)/r^7$ be-

comes small. Therefore, the second term of eq. (A7) becomes negligible. Consequently, from eq. (A1) the voltage V generated by moving the sample is given by

$$V=[(3NSa\omega xM)/(4\pi r^5)]\sin(\omega t)=V_0\sin(\omega t),$$

$$V_0=(3NSa\omega xM)/(4\pi r^5)=C(x/r^5) \qquad (A8)$$

and

$$C=3NSa\omega M/4\pi .$$

The amplitude V_0 is described by the geometrical factor and the characteristics of the detection coil, as well as by ω, a, and M. If the magnetization M is vibrated with constant ω and a, the amplitude of the electro-motive force V is proportional to the sample magnetic moment M. This paper is concerned with the discussion of the geometrical factor (x/r^5) in the amplitude of V_0 in order to reduce the influence due to sample mispositioning.

We will only be concerned with the four-coil detection system from now on. Figure A2(a) shows this multiple-coil configuration. The four coils have a series connection, where the Nos. 2 and 3 coils in Fig. 2(a) are connected in the opposite wind to Nos. 1 and 4 coils in order to obtain a net output signal. Thus, when the mean position of the magnetic moment is taken as the origin, the amplitude of the voltage induced in the four detection coils becomes

$$V_0(\text{total})=(4Cx_0)/{r_0}^5\equiv W, \qquad (A9)$$

where a new simple notation, W, is introduced.

In order to make further progress, it is necessary to obtain the induced voltage when the magnetic moment M is displaced from the origin by a small amount $(\Delta x,\Delta y,\Delta z)$ at the same time. For example, the amplitude of the induced voltage in the number–1 detection coil is

$$V_1(\Delta x,\Delta y,\Delta z)=C(x_0-\Delta x)/[(x_0-\Delta x)^2+(y_0-\Delta y)^2+(\Delta z)^2]^{5/2}$$

$$\fallingdotseq C[(x_0-\Delta x)/{r_0}^5]\cdot[1-(5/2)P+(35/8)Q], \qquad (A10)$$

where, the higher order of displacement is neglected, and P and Q are, respectively, defined as

$$P=[(\Delta x)^2+(\Delta y)^2+(\Delta z)^2-2(\Delta x)x_0-2(\Delta y)y_0]/({r_0}^2) \qquad (A11)$$

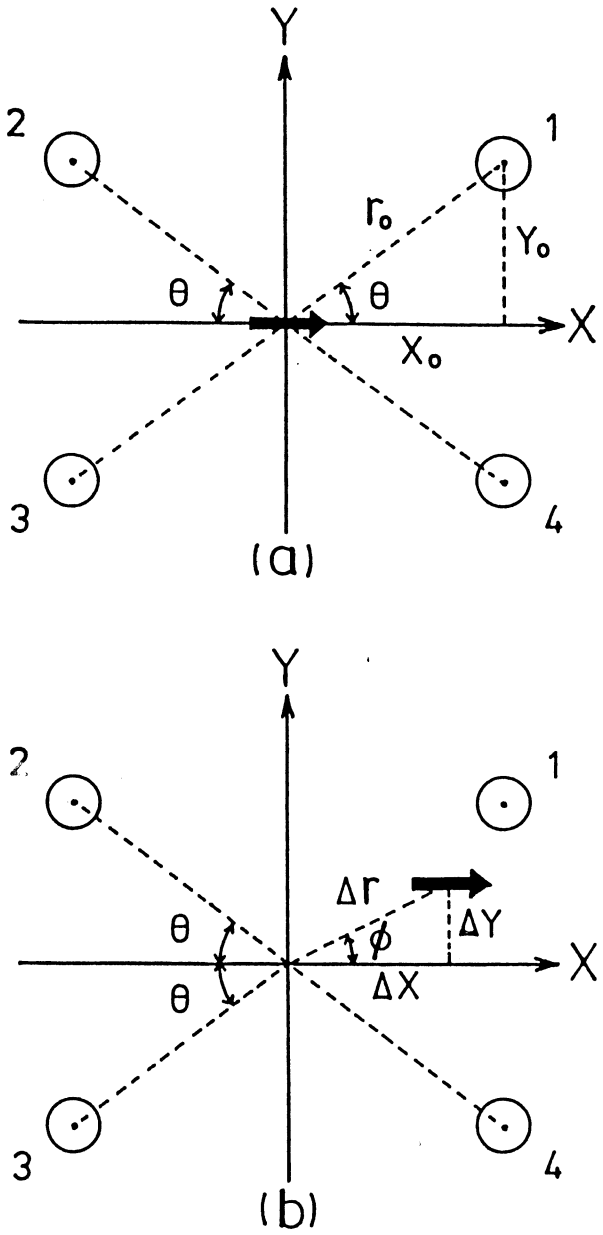

Fig. A2(a) A detection coil configuration consisting of four identical N-turn coils. The cross sections of four coils in this multiple-coil arrangement are shown. The sample having a magnetic moment M, indicated by the heavy arrow, is vibrated along the z-direction. The angle θ is measured from the x-axis.

(b) A situation in which the mean position of the sample magnetic moment originally at the origin is displaced by a small amount $\Delta r(\Delta x,\Delta y,0)$ due to the sample mispositioning. The sample still keeps vibrating along the z-direction. The angle ϕ is the angle between the x-axis and the Δr.

and

$$Q=[4(\Delta x)^2x_0^2+8(\Delta x)(\Delta y)x_0y_0+4(\Delta y)^2y_0^2]/(r_0^4). \tag{A12}$$

Then, the amplitude in the induced voltage is given by

$$V(\Delta x,\Delta y,\Delta z)=V_1+V_2+V_3+V_4$$

$$=W[1+K_x(\Delta x/r_0)^2+K_y(\Delta y/r_0)^2+K_z(\Delta z/r_0)^2]. \tag{A13}$$

To bring eq. (A13) into a manageable form, we introduced the following definitions:

$$K_x=-(5/2)[3-7(x_0/r_0)^2],$$

$$K_y=-(5/2)[1-7(y_0/r_0)^2] \tag{A14}$$

and

Table A1 Numerical values of K_ϕ, defined in text, as a function of ϕ for several detection coil arrangements characterized by θ (see Fig. A2).

ϕ(°): sample position	θ(°): detection coil configuration					
	0	30	36.7	45	60	90
0	10.0	5.63	3.75	1.25	−3.13	−7.50
15	9.16	5.37	3.75	1.58	−2.20	−5.99
30	6.88	4.69	3.75	2.50	0.313	−1.88
45	3.75	3.75	3.75	3.75	3.75	3.75
60	0.625	2.81	3.75	5.00	7.19	9.37
75	−1.66	2.13	3.75	5.92	9.70	13.5
90	−2.50	1.88	3.75	6.25	10.6	15.0

$K_z=-(5/2)$.

Furthermore, let us introduce the angle ϕ and Δr as (see Fig. A2(b))

$$\Delta x=(\Delta r)\cos\phi$$

and

$$\Delta y=(\Delta r)\sin\phi\,. \tag{A15}$$

Also, let

$$K_\phi=K_x(\cos\phi)^2+K_y(\sin\phi)^2. \tag{A16}$$

Then, eq. (A13) can be rewritten in terms of these definitions

$$V(\Delta x,\Delta y,\Delta z)=W[1+K_\phi(\Delta r/r_0)^2+K_z(\Delta z/r_0)^2] \tag{A17}$$

as well as

$$V(\Delta x,\Delta y,0)=W[1+K_\phi(\Delta r/r_0)^2], \tag{A18}$$

$$V(0,0,\Delta z)=W[1+K_z(\Delta z/z_0)^2]. \tag{A19}$$

As a result, if the magnetic moment is displaced in the x–y plane, the characteristics of the induced voltage is completely determined by K_ϕ (having a simply reduced parameter of angle ϕ).

Next, the results of a numerical calculation of K_ϕ will be shown. Table A1 gives a list of the numerical values for K_ϕ as a function of the angle ϕ, in which the various detection coil arrangements are characterized by the angle θ indicated in Fig. A2(a). Our final objective concerning this argument is to determine a relevant angle θ in order to minimize the undesirable effects due to any sample mispositioning which comes from the existence of Δx and Δy. Here, it should be noted that there exist a characteristic angle $\theta=36.7$ degree in which K_x is equal to K_y; then, the magnitude K_ϕ is independent of the angle ϕ, as can be seen in Table A1. The angular dependence of K_ϕ is shown in Fig. A3. The detection coil configuration having the characteristic angle $\theta=36.7$ degrees gives a constant magnitude of $K_\phi=3.75$. All the other detection coil configurations have a larger value for K_ϕ in a certain region of angle ϕ. These results lead us to a significant conclusion. Namely when the magnetic moment M is displaced in the x–y plane owing to sample mispositioning, the detection-coil configuration should be set at $\theta=36.7$ degrees in order to reduce any mispositioning influence.

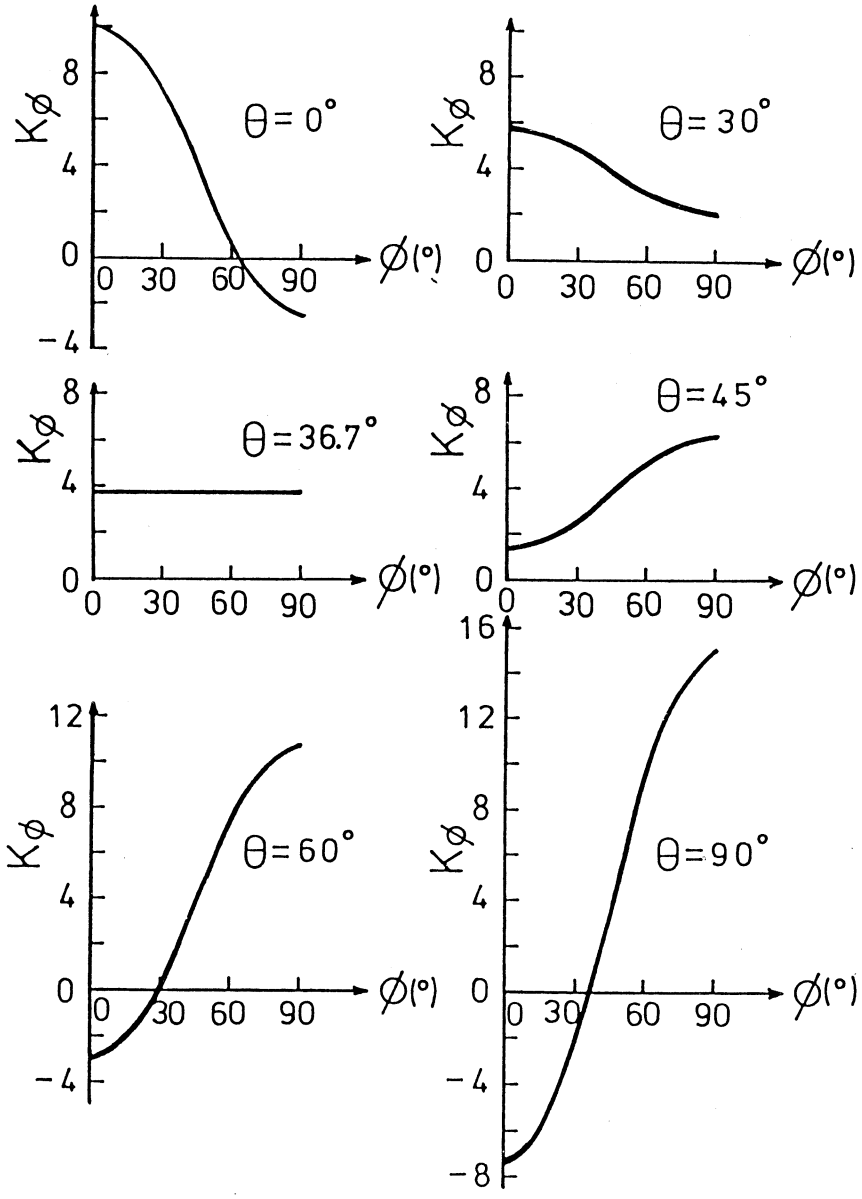

Fig. A3 The characteristic feature of the angular dependence of K_ϕ for the 6 different detection coil arrangements.If the detection coils are set up to have $\theta = 36.7$ degrees, it can be seen that K_ϕ has a constant value of 3.75 for any displacement angle ϕ. For all the other coil configurations, the magnitude of K_ϕ is larger than 3.75 in a certain region of the displacement angle ϕ.

As a next approach, the amount of the relative output signal from a four-coil detection system, with the relevant angle $\theta = 36.7$ degree, is obtained in Table A2. The actual feature of the relative output signal is seen in Fig. A4. If the angle θ is chosen to be 36.7 degree, the relative output signal gives less than 1 % change in the output signal within the range of the 5 % in the relative displacement.

Since the z–axis is the direction of motion of the sample and the sample position is determined by a vibrating rod, it is unlikely that the displacement, itself, along the z-direction would arise.

Table A2 The numerical values of the relative output signal from a four-coil detection system when $\theta = 36.7$ degree. The sample positions are given by $\Delta r/r_0$ and $\Delta z/r_0$.

Displacement in the x-y plane		Displacement along the z-direction	
$\frac{\Delta r}{r_0}$	$\frac{V(\Delta x, \Delta y, 0)}{V(0,0,0)}$	$\frac{\Delta z}{r_0}$	$\frac{V(0,0,\Delta z)}{V(0,0,0)}$
0	1	0	1
0.01	1.0004	0.01	0.9998
0.02	1.0015	0.02	0.9990
0.03	1.0034	0.03	0.9978
0.04	1.0060	0.04	0.9960
0.05	1.0094	0.05	0.9938
0.06	1.0135	0.06	0.9910
0.07	1.0184	0.07	0.9878
0.08	1.0240	0.08	0.9840
0.09	1.0304	0.09	0.9798
0.10	1.0375	0.10	0.9750

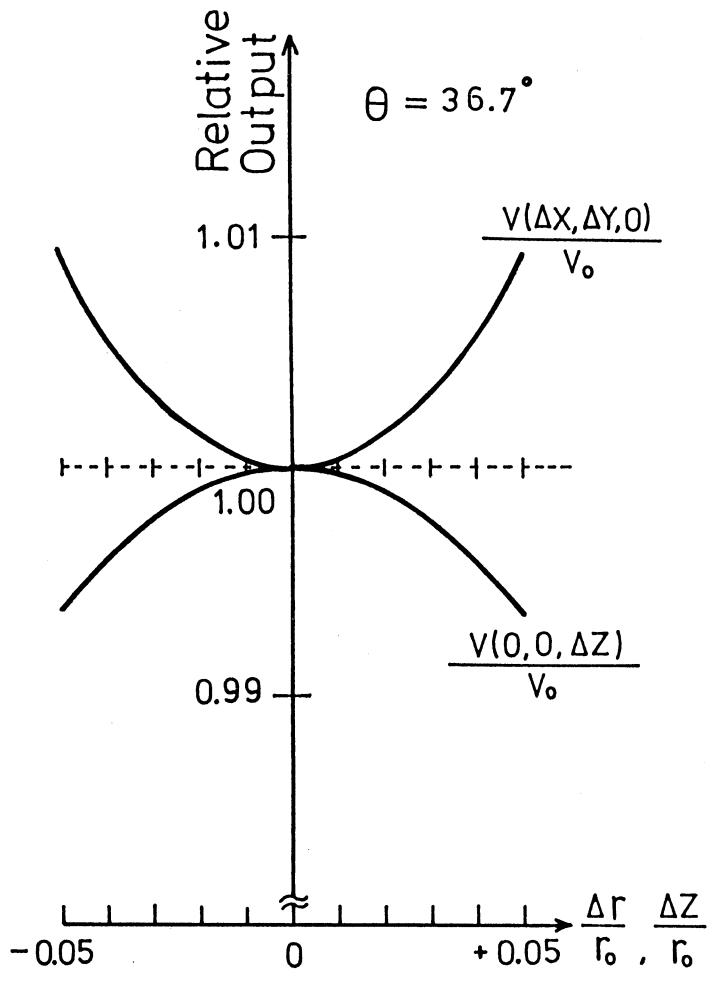

Fig. A4 The relative output signal of the four-coil detection system as a function of the sample position. The angle between r_0 and the x-axis is 36.7 degree, that is the the best angle to reduce undesirable sample mispositioning effects.

From the preceding results, the discussion of the relative sensitivity in the output voltage for the displacament in the x–y plane has significant importance in the actual experimental situation; this is because the problem for the z–direction displacement is less significant. Consequently, if the relevant angle, $\theta = 36.7$ degrees is chosen, any undesirable influence due to sample mispositioning and departures from constructional ideality can be minimized.

References

1) B. E. Argyle, S. H. Charap and E. W. Pugh: Phys. Rev. *132*, 2051 (1963).
2) E. W. Pugh and B. E. Argyle: Suppl. J. Appl. Phys. *33*, 1178 (1962).
3) H. E. Nigh, S. Legvold and F. H. Spedding: Phys. Rev. *132*, 1092 (1963).
4) W. D. Corner, W. C. Roe and K. N. R. Taylor: Proc. Phys. Soc. (London) *80*, 927 (1962).
5) C. D. Graham: J. Appl. Phys. Suppl., *34*, 1341 (1963).
6) S. Nagata, S. Ebisu and S. Taniguchi: Physica B (Utrecht) 150, 423 (1988).
7) S. Nagata, S. Ebisu, E. Fujita, M. Miyazaki and S. Taniguchi: Jpn. J. Appl. Phys. Suppl. *26-3*, 825 (1987).
8) H. W. White, B. J. Beaudry, P. Burgardt, S. Legvold and B. N. Harmon: AIP Conf. (USA) No. *29*, 329 (1976).
9) F. Keffer: *Handbuch der Physik* Vol. *18/2*, p. 1 (Springer-Verlag, edited by H.P.J. Wijn, New-York, 1966).
10) S. N. Kaul: Phys. Rev. *B27*, 5761 (1983).
11) C. Kittel: *Quantum theory of solids*, p 49 (John Wiley & Sons, Inc., New York・London 1963).
12) S. Nagata, M. Miyazaki, E. Fujita and S. Taniguchi: Cryogenic Engineering (Teion-Kougaku) *21*, 295 (1986) [in Japanese].
13) S. Nagata, E. Fujita, S. Ebisu and S. Taniguchi: Jpn. J. Appl. Phys. *26*, 92 (1987).
14) S. Nagata and S. Taniguchi: Solid State Physics (Kotai Butsuri) *21*, 877 (1986) [in Japanese].
15) S. Chikazumi: *Physics of Magnetism*, p 274 (Robert E. Krieger Pub., Huntington, New York 1978).
16) J. F. Elliott, S. Legvold and F. H. Spedding: Phys. Rev. *91*, 28 (1953).